arXiv:cond-mat/9809113v1 [cond-mat.str-el] 7 Sep 1998

Vortex, skyrmion and elliptical domain wall textures in the two-dimensional Hubbard model

G. Seibold
Institut für Physik, BTU Cottbus, PBox 101344, 03013 Cottbus, Germany

(February 1, 2008)

The spin and charge texture around doped holes in the two-dimensional Hubbard model is calculated within an unrestricted spin rotational invariant slave-boson approach. In the first part we examine in detail the spin structure around two holes doped in the half-filled system where we have studied cluster sizes up to 10×10. It turns out that the most stable configuration corresponds to a vortex-antivortex pair which has lower energy than the Néel-type bipolaron even when one takes the far field contribution into account. We also obtain skyrmions as local minima of the energy functional but with higher total energy than the vortex solutions. Additionally we have investigated the stability of elliptical domain walls for commensurate hole concentrations. We find that (i) these phases correspond to local minima of the energy functional only in case of partially filled walls, (ii) elliptical domain walls are only stable in the low doping regime.

PACS numbers: 71.27.+a,71.10.Fd,75.10.-b,75.60.Ch

I. INTRODUCTION

The description of inhomogeneous charge and spin phases in the Hubbard model it a topic of current interest, mainly because it is now generally accepted that the high-T$_c$ compounds, at least in the underdoped regime, are intrinsic electronically inhomogeneous systems. A powerful tool for the investigation of such inhomogeneous electronic states is the unrestricted Hartree-Fock (HF) scheme which allows for the diagonalization of reasonable cluster sizes. Recently an extension of this approach based on the Gutzwiller wave function [1] has shown to significantly improve the HF solutions which strongly underestimate the attraction between charge carriers. In this paper we extend the approach of Ref. [1] to include transversal spin degrees of freedoms which permits the description of coplanar and three-dimensional inhomogeneous spin textures.

Among coplanar spin structures homogeneous spiral solutions have been studied by a large variety of methods (see e.g. [2,3]) which show that a small amount of holes doped into the half-filled system leads to a $\mathbf{Q} \sim (1,1)$ spiral phase which changes its direction to $\mathbf{Q} \sim (1,0)$ above some critical concentration. Relaxing the constraint of a homogeneous charge distribution the formation of coplanar, vortexlike phases has been investigated in Ref. [4] using an unrestricted HF approach. These are configurations where the antiferromagnetic (AF) spin order rotates by multiples of 2π around the localized hole. Due to this twist in the magnetization their energy increases $\sim ln(L^2)$ which implies their instability in large clusters.

A three-dimensional spin texture which is known to be topologically stable is the skyrmion as a solution of the O(3) non-linear σ-model [6]. It has been studied by several authors also for an AF background [7,8] mainly concentrating on small clusters.

However, it is still controversal wether skyrmion solutions exist also on discrete lattices. Whereas unrestricted HF theory for the 2-d Hubbard model predicts the decay of skyrmions into conventional spin-polarons [4], exact diagonalization studies of a small cluster within the tJ-model Ref. [9] seem to support their existence even when one takes the contribution of the skyrmion far field into acount. Within our slave-boson approach we will show below that skyrmions textures are stable solutions of the discrete two-dimensional Hubbard model, when the system is doped with two holes away from half-filling.

Connected with the discovery of static stripe order in La$_2$NiO$_4$ and La$_{1.48}$Nd$_{0.4}$Sr$_{0.12}$CuO$_4$ [10,11] a lot of work has been done in order to understand the different domain wall structures in these compounds [12–15]. Whereas in the Ni-doped compounds one finds the stripes along the diagonal with one hole per Ni-site the charge and spin order in the Nd-doped cuprates is along the copper-oxygen bond direction with one hole per every second copper site only. Since half-filled horizontal walls are at odds with HF calculations the inclusion of correlations turns out to be a necessary ingredient for the study of domain walls in these systems [14,15]. In addition long-range Coulomb interactions can play an important role in stabilizing half-filled vertical stripes [14].

Based on a Landau free-energy analysis of coupled charge and spin-density-wave order parameters it has been shown in Ref. [16] that within some region of parameter domain walls may have a spiral component. Whereas this type of ordering is not observed in the Ni-oxides, some spiral contribution cannot be rigorously excluded to be present in the Nd-doped compounds [11]. According to our analysis presented below, elliptical stripes are not stable for concentrations around 1/8 but may be formed in the very low doping limit.

The rest of the paper is organized as follows: In Sec. II we give a detailed description of the formalism, in Sec. III we present the results for vortex, skyrmion and elliptical domain wall solutions respectively, and in Sec. IV we summarize our conclusions.

II. MODEL AND FORMALISM

We consider the two-dimensional Hubbard model on a square lattice, with hopping restricted to nearest neighbors (indicated by the bracket $< i,j >$)

$$H = -t \sum_{<ij>,\sigma} c^\dagger_{i,\sigma} c_{j,\sigma} + U \sum_i n_{i,\uparrow} n_{i,\downarrow} \tag{1}$$

where $c^{(\dagger)}_{i,\sigma}$ destroys (creates) an electron with spin σ at site i, and $n_{i,\sigma} = c^\dagger_{i,\sigma} c_{i,\sigma}$. U is the on-site Hubbard repulsion and t the transfer parameter. For the calculations in Sec. III we take t=1. In the following we use a spin-rotation-invariant form [17] of the slave-boson representation introduced by Kotliar and Ruckenstein in Ref. [18]. The subsidiary boson fields $e^{(\dagger)}_i$, $d^{(\dagger)}_i$ stand for the annihilation (creation) of empty and doubly occupied sites, respectively, whereas the matrix

$$\mathbf{p_i} = \begin{pmatrix} p_{i,\uparrow} & \frac{1}{\sqrt{2}}(p_{i,x} - ip_{i,y}) \\ \frac{1}{\sqrt{2}}(p_{i,x} + ip_{i,y}) & p_{i,\downarrow} \end{pmatrix} \tag{2}$$

represents the case of a singly occupied site. Since we consider the mean-field limit all boson operators will be approximated as numbers. Besides the completeness condition

$$e_i^2 + tr(\mathbf{p}^*_{\mathbf{i},\mu} \mathbf{p}_{\mathbf{i},\mu}) + d_i^2 = 1 \tag{3}$$

the boson fields are constrained by the following relations

$$tr(\tau_\mu \mathbf{p}^*_\mathbf{i} \mathbf{p}_\mathbf{i}) + 2\delta_{\mu,0} d_i^2 = \sum_{\sigma\sigma'} c^\dagger_{i,\sigma} (\tau_\mu)_{\sigma\sigma'} c_{i,\sigma'} \tag{4}$$

where $\tau_{\mu=\mathbf{1},\mathbf{2},\mathbf{3}}$ are the Pauli spin matrices and $\tau_{\mu=\mathbf{0}} \equiv \mathbf{1}$.

Then, in the physical subspace defined by Eqs. (3,4) the Hamiltonian (1) takes the form

$$\tilde{H} = -t \sum_{<ij>,\sigma\sigma_1\sigma_2} z^*_{i,\sigma\sigma_1} c^\dagger_{i,\sigma_1} c_{j,\sigma_2} z_{j,\sigma_2\sigma} + U \sum_i d_i^2 \tag{5}$$

where

$$\mathbf{z_i} = \mathbf{L_i}(e_i \mathbf{p_i} + \tilde{\mathbf{p}}_\mathbf{i} d_i) \mathbf{R_i} \tag{6}$$

$$\mathbf{L_i} = \left[(1-d_i^2)\mathbf{1} - \mathbf{p}^*_\mathbf{i} \mathbf{p_i}\right]^{-1/2} \tag{7}$$

$$\mathbf{R_i} = \left[(1-e_i^2)\mathbf{1} - \tilde{\mathbf{p}}^*_\mathbf{i} \tilde{\mathbf{p}}_\mathbf{i}\right]^{-1/2} \tag{8}$$

The matrices $\mathbf{L_i}$ and $\mathbf{R_i}$ guarantee the correct behavior in the limit $U \to 0$ within the mean-field approximation and $\tilde{\mathbf{p}}_\mathbf{i} = \hat{T} \mathbf{p_i} \hat{T}^{-1}$ is the time-reversal transformed of $\mathbf{p_i}$.

The matrix elements of $\mathbf{z_i}$ can be calculated by transforming to a diagonal representation for the $\mathbf{p_i}$ (see Appendix). The resulting effective one-particle Hamiltonian describes the dynamics of particles which upon hopping between sites are subjected to a modulation of their spin amplitude and spin direction, respectively. It can be diagonalized by the transformation

$$c_{i,\sigma} = \sum_k \Phi_{i,\sigma}(k) a_k \tag{9}$$

where the orthogonality of the transformation requires

$$\sum_{i,\sigma} \Phi^*_{i,\sigma}(k) \Phi_{i,\sigma}(q) = \delta_{kq}. \tag{10}$$

Given a system with N_{el} particles we finally obtain for the total energy

$$E_{tot} = -t \sum_{<ij>,\sigma\sigma_1\sigma_2} z^*_{i,\sigma\sigma_1} z_{j,\sigma_2\sigma} \sum_{k=1}^{N_{el}} \Phi^*_{i,\sigma_1}(k) \Phi_{j,\sigma_2}(k) + U \sum_i d_i^2 \tag{11}$$

which has to be evaluated within the constraints (3,4, 10). This is achieved by adding these constraints quadratically to Eq. (11) following the procedure already applied in the Gutzwiller limit [1]. The resulting energy functional then has to be minimized with respect to the fermionic and bosonic fields which is most conveniently done by using a standard conjugate gradient algorithm since the gradients of the energy functional can be calculated analytically. In order not to end up in pathological side minimas we have generally started the minimization from an HF Ansatz for the amplitudes $\Phi_{i,\sigma}(k)$.

III. RESULTS

Since in a previous publication [1] the unrestricted slave-boson approximation has been already applied to the description of collinear spin structures, we will restrict here to textures with two- and three dimensional spin ordering. In this section we discuss the spin structure of vortex, skyrmion and elliptical domain wall textures which turn out to be stable energy minima within our slave-boson approach. Obviously on finite lattices one has to use open boundary conditions in order to describe higher dimensional spin structures and the cluster sizes we are considering in the following are ranging from 6×6 up to 10×10.

The incorporation of transversal spin degrees of freedom allows for the definition of spin currents $\nabla \mathbf{j} = -\partial_t \mathbf{S}$. The flow direction of these currents is along the bonds of the lattice, however, they are additionally vectorial in spin space and within the present approach we obtain for the i-th component of the spin current flowing between sites $< nm >$:

$$j^i_{nm} \sim Im \sum_{\sigma_1\sigma_2\sigma_3\sigma_4} \sum_{k=1}^{N_{el}} \Phi^*_{n,\sigma_1}(k)\tau^i_{\sigma_1\sigma_2} z^*_{n,\sigma_3\sigma_2} z_{m,\sigma_4\sigma_3} \Phi_{m,\sigma_4}(k) \tag{12}$$

where τ^i are the Pauli matrices and the hopping factors $z_{n,\sigma\sigma'}$ are defined in Eq. (6). The i-th component of $\mathbf{j}_{nm}$ can be thought of as measuring the spin-twist in the orthogonal directions $l, k \neq i$ so that the total current components j^i_n, which are plotted in the results, visualize the direction of maximal twist in the spin components $lk \neq i$ at lattice site n.

A. Vortex States

The structure of vortex solutions, where the magnetization rotates in a plane by some multiples of 2π around the localized holes, has already been studied in Ref. [4] within unrestricted HF theory. We also obtain vortex states as local minima of the energy functional (11), where the total energy is about $5\% - 10\%$ lower than in the HF approach, depending on lattice size and on-site repulsion U. However, for one hole away from half-filling vortex solutions are always higher in energy than the conventional Néel ordered spin polaron. Moreover, their total energy increases logarithmically with the cluster size as a consequence of the twist between neighboring magnetization vectors in agreement with Ref. [4].

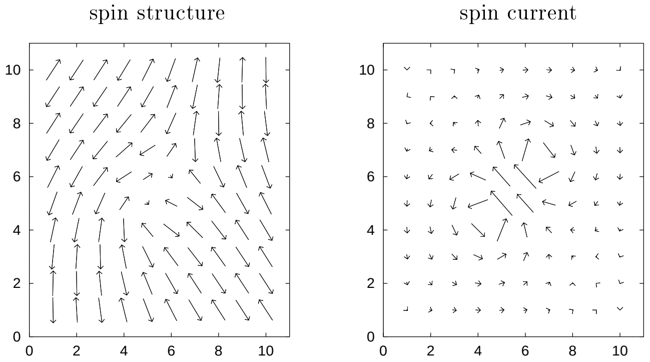

FIG. 1. Spin structure and spin currents for a vortex-antivortex pair on a 10×10 lattice. The Hubbard on-site repulsion is $U = 10t$.

This logarithmic divergency can be compensated when two holes form a vortex-antivortex pair. According to our calculations the vortex cores are located at the center of diagonally next nearest neighbor plaquettes, thus separated by the plaquette where the two holes are localized. Fig. 1 shows the spin structure and spin current of such a vortex-antivortex pair on a 10×10 cluster and $U = 10t$. All the spins lie in the xy-plane which means that only the z-component of the spin current has a non zero contribution. The spin field of this texture can be described by

$$\mathbf{S}_i = S_0 e^{i\mathbf{Q}\mathbf{R}_i}[\cos(\phi_1 - \phi_2)\mathbf{e_x} + \sin(\phi_1 - \phi_2)\mathbf{e_y}] \tag{13}$$

where ϕ_1, (ϕ_2) refer to the angles between x-axis and the vectors connecting vortex (antivortex) core and site $\mathbf{R}_i$. The AF wave vector is denoted by $\mathbf{Q}$.

Concerning the stability of the vortex-antivortex pair we obtain for the 10×10 cluster and $U = 10t$ a binding energy of $E^b = -0.047t$ with respect to the Néel type bipolaron. Taking into account the far field energy, calculated within the xy-model for the spin structure Eq. (13) and an exchange constant of $J = 4t^2/U = 0.4t$ still results in a negative binding energy of $E^b_{tot} = -0.016t$.

We note that the absolute value of E^b_{tot} slightly decreases for smaller cluster sizes since the boundary spins do not properly adjust to the solution Eq. (13). One can therefore safely conclude that vortex-antivortex pairs are also stable in the thermodynamic cluster limit.

B. Skyrmions

On a discrete 2-dimensional AF lattice the spin structure of skyrmions, originally obtained as solutions of the O(3) non-linear σ-model [6], has the form [7,8]

$$\begin{aligned} S_x &= (-1)^{i_x+i_y} \frac{\lambda i_x}{i_x^2 + i_y^2 + \lambda^2} \\ S_y &= (-1)^{i_x+i_y} \frac{\lambda i_y}{i_x^2 + i_y^2 + \lambda^2} \\ S_z &= (-1)^{i_x+i_y} \frac{1}{2} \frac{i_x^2 + i_y^2 - \lambda^2}{i_x^2 + i_y^2 + \lambda^2} \end{aligned} \tag{14}$$

where λ denotes the core size of the skyrmion and its center is located at $i_x = i_y = 0$.

In order to enhance convergence we initialized our minimization procedure with (non self-consistent) HF wave functions corresponding to the spin fields Eqs. (14).

Despite intensive search we could not obtain skyrmion states for one hole doped in the half-filled system. These solutions always converged towards a spin-polaron embedded into a collinear AF Néel state as already observed in Ref. [4].

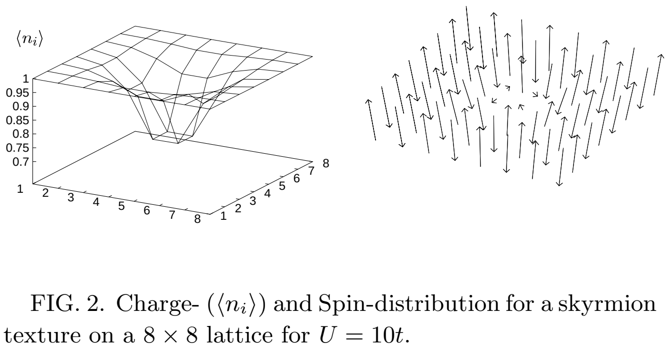

FIG. 2. Charge- ($\langle n_i \rangle$) and Spin-distribution for a skyrmion texture on a 8×8 lattice for $U = 10t$.

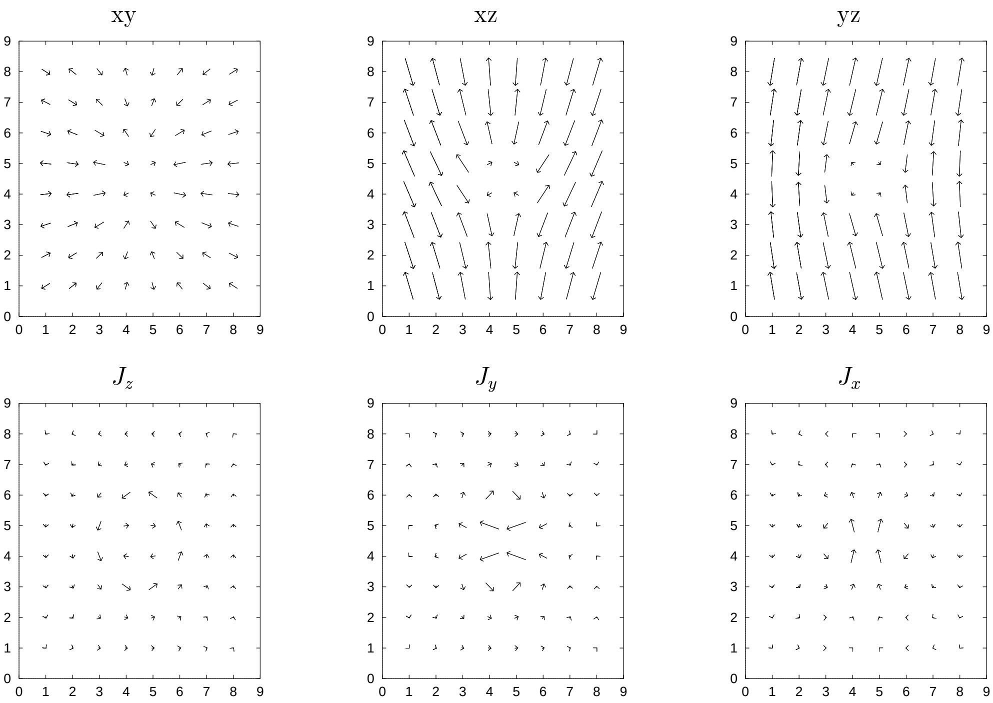

FIG. 3. xy-, yz- and xz-projections of the spins together with the respective spin currents for the skyrmion shown in Fig. 2

The situation changes when removing two particles from the half-filled system. Fig. 2 displays the charge- and spin structure in case of 62 particles on a 8×8 lattice for $U = 10t$. The two holes then are localized on a $2{\times}2$ plaquette at the skyrmion center and in their vicinity spins show a remarkable deviation from the z-direction. This is more easily seen in Fig. 3 where we have plotted the xy-, xz- and yz- spin projections, respectively, together with the corresponding spin currents. The xy-spin components rotate by 360° around the skyrmion center resulting in a circular spin current for j^z. However, all current components strongly decay for sites far away from the skyrmion center indicating that the core size parameter λ is small. Upon fitting our solutions to the skyrmion field Eq. (14) we obtain $\lambda \approx 0.7$ for $U = 10t$ and cluster sizes 6×6, 8×8 and 10×10, respectively. This already indicates that the skyrmion state should survive the limit of large clusters.

To assess the question of stability in more detail we have also calculated the total energy using skyrmionic boundary conditions [9]. These are defined through an exchange field $J\mathcal{S}(R, \lambda)$ to which the spins at the boundary are coupled and $\mathcal{S}(R, \lambda)$ has the form of Eq. (14). For the exchange constant we take the strong-coupling value of the Hubbard model $J = 4t^2/U$. The total energy then is evaluated as a function of λ and in the result we substract the energy contribution of the exchange field. This energy has to be compared with the corresponding value of a collinear bipolaron where two holes are localized on neighbored sites within the Néel ordered system. The results are plotted in Fig. 4 again for $U = 10t$ and three different cluster sizes. As can be seen all curves display a clear minimum at some value of λ indicating the presence of a stable skyrmion solution with a significant lower energy than the collinear bipolaron. It should be mentioned that these minima for the corresponding one-hole doped systems are always at $\lambda = 0$, i.e. the configuration of a conventional spin-polaron. From the results shown in Fig. 4 one further sees that a lowering of energy with respect to the AF bipolaron is already obtained for $\lambda = 0$ indicating that despite the imposed Néel boundaries the system has a skyrmion like core. This energy shift increases with the system size since the central spins of large lattices can more properly adjust to the skyrmion state. From the fact that the $\lambda = 0$ results for the 8×8 and 10×10 coincide within the numerical error we conclude that also in the thermodynamic limit the skyrmion solution should survive. Also plotted in Fig. 4 with filled symbols are the energy differences between bipolarons and skyrmions calculated with open boundary conditions. As already mentioned one obtains the same core parameter λ for all three cluster sizes which agrees with the position of the minimum of the solid line ($10{\times}10$ system). Also this feature demonstrates that our largest cluster should already correctly describe the skyrmion structure of infinite clusters. Since the skyrmion on small lattices is very much influenced by the boundary conditions the minimum of the dotted curve (6×6 cluster) is shifted to a higher value of $\lambda \approx 1$.

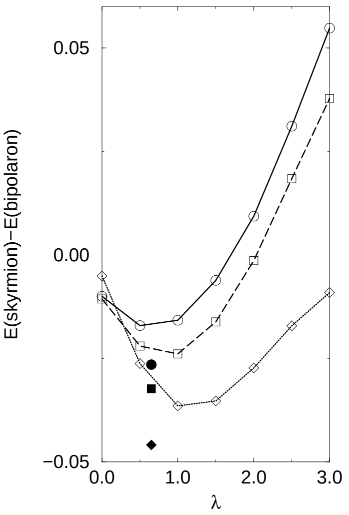

FIG. 4. Total energy of a two-hole-skyrmion with respect to the energy of a Néel-type bipolaron as a function of the skyrmion core size parameter λ. The boundary spins have been coupled to the skyrmion solution Eq. (14) via a mean-field exchange field. Solid line and circles: 10×10 lattice; Dashed line and squares: 8×8 lattice; Dotted line and diamonds: 6×6 lattice. The full symbols mark the energies for open boundary conditions. $U = 10t$.

In order to compare the stability of skyrmion states with the vortex-antivortex solutions, one has to take into account the far field contribution to the total energy. Considering again a 10×10 system and $U = 10t$ the skyrmion binding energy with respect to the Néel-type bipolaron (cf. Fig. 4) is $E^b_{tot} = -0.0265t$. Including the far field energy (taking again $J = 0.4t$) one obtains $E^b_{tot} = -0.0071t$ which is approximately half the value of the vortex-antivortex binding energy.

C. Elliptical domain walls

The possibility that charge-spin coupling in correlated systems may induce the formation of elliptical domain walls was proposed by an analysis of the Landau free-energy functional for coupled charge- and spin density waves [16]. These are coplanar spin structures where the spin components in the first harmonic are modulated as

$$\begin{aligned} S_x(\mathbf{r}) &= S_0 e^{i\mathbf{Q}\mathbf{r}} \cos(\alpha)\cos(\mathbf{q}\mathbf{r}) \\ S_y(\mathbf{r}) &= \pm S_0 e^{i\mathbf{Q}\mathbf{r}} \sin(\alpha)\sin(\mathbf{q}\mathbf{r}) \end{aligned} \qquad (15)$$

The eccentricity of the elliptical domain wall is determined by α and $\mathbf{Q}, \mathbf{q}$ correspond to the wave vectors of commensurate AF and the domain wall periodicity, respectively. The case $\alpha = \pi/4$ describes an ideal spiral solution whereas $\alpha = 0$ reduces the spin structure to a collinear 'classical' domain wall.

We have used (non-self consistent) HF states corresponding to Eq. (15) as starting fields for our minimization for different values of α. Only vertical domain walls have been considered and periodic boundary conditions where applied in the x- and y-direction, respectively. In case of a completely filled domain wall (i.e. one hole per site along the wall) we only found the collinear solutions whereas coplanar structures become stable for half-filled walls.

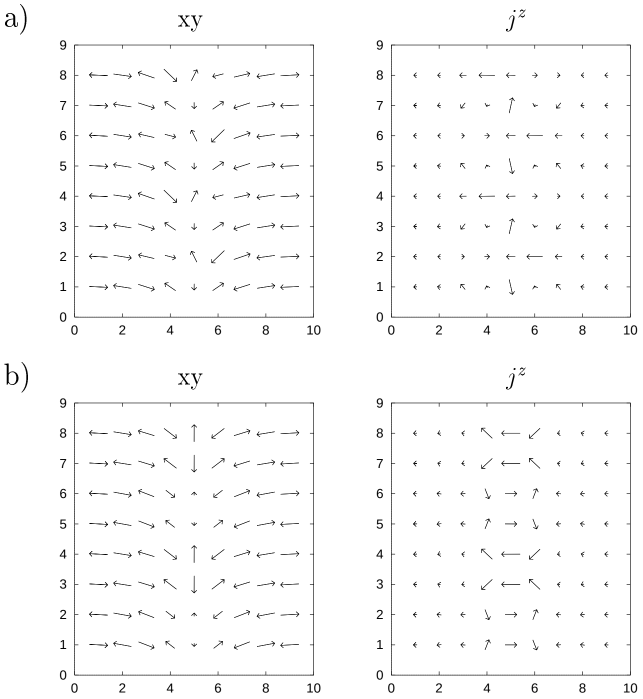

FIG. 5. Two possible spin structures for elliptical domain walls together with the corresponding spin currents. The on-site repulsion is $U = 6t$ and periodic boundary conditions in x- and y-direction have been used. Shown are the results for a 9×8 lattice doped with 4 holes.

This is shown in Fig. 5 for a 9×8 lattice with 68 particles where we plot two kinds of possible spin structures which are local minima of the energy functional Eq. (11). Also shown are the respective spin currents (only z-components since the magnetization vector is completely in the xy-plane). Spin fields and currents display a quadrupled structure along the wall which is a necessary condition for stability within any mean-field approach [13]. Due to the stripe charge structure the current flows are more complex than for the elliptical solution Eq. (15) which predicts currents flowing in a single direction orthogonal to the wall. Instead we observe also currents along the wall (Fig. 5a) and a vortex-antivortex structure in Fig. 5b.

Although the elliptical stripes are local minima of the energy functional Eq. (11) they are slightly higher in energy ($\approx 5\%$) than collinear domain walls. These have been shown to correspond to the ground state when one takes long-range Coulomb interactions into account [14]. However, we do not expect significant differences of a long-range contribution to collinear and elliptical stripe solutions.

The structures shown in Fig. 5 correspond to systems with hole doping 1/18 and we could not obtain elliptical solutions for higher doping. However, one can also study the very low doping limit upon using open boundaries in the x-direction. Indeed in this case elliptical half-filled stripes become favored with repect to collinear domain walls for not too large values of the on-site repulsion U ($< 9t$).

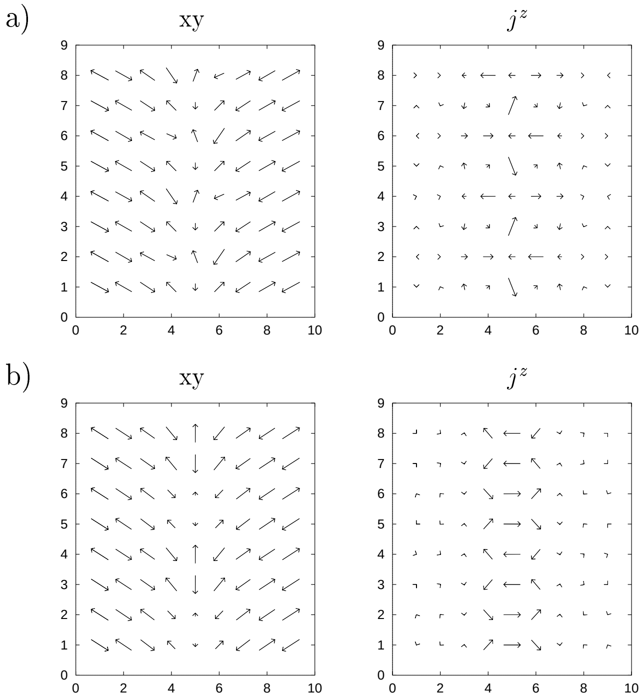

FIG. 6. The same as in Fig. 5 but now for open boundaries in x-direction.

In Fig. 6 we show the same spin structures as in Fig. 5 but for open boundaries in x-direction. The main difference between these two figures concerns the angle of spin rotation Θ across the domain wall which is only $\approx 3/4$ of the expected value of π according to Eq. (15). This is due to the fact that the system now can acquire a state which has zero total spin current, whereas for periodic boundaries the spiral component always requires a net flow in x-direction.

However, since for a regular array of stripes the charge periodicity and the spin modulation have to be related by $k^{charge} = 2k^{spin}$ [16] the domain wall induced kink type spin rotation has to be supplemented by an additional spiral field. Assuming an exponential relaxation of the spin rotation from Θ to π by this spiral field gives an additional energy per site of $\Delta E \approx \rho_s(\pi - \Theta)^2\lambda/L$ where $\rho_s = JS^2$ is the spin stiffness, λ defines the length scale of relaxation and L is the stripe separation. Consequently this additional energy can become small enough in the low doping regime so that elliptical stripe configurations are more stable than collinear solutions for small hole concentrations.

IV. CONCLUSION

Summarizing, we have presented the structure of spin textures which we obtained by applying an unrestricted slave-boson mean-field approximation in its spin-rotation invariant form to the 2D Hubbard model. This approach is suited for calculating the charge and spin distribution of electrons (holes) in inhomogeneous and strongly correlated systems since it incorporates correlation effects beyond the standard unrestricted HF theory. These correlation effects turn out to be especially important for the interaction among holes in the 2-D Hubbard model where the HF approximation strongly underestimates their attractive potential [1].

Including the effect of transversal degrees of freedom we have shown that within our slave-boson mean-field approach two holes in the half-filled two-dimensional Hubbard model are bound by forming a vortex-antivortex pair, oriented along the diagonal direction. This texture has significantly lower energy than a conventional collinear bipolaron, also when the far field contribution is taken into account. Additionally we have found that skyrmion states can be stable even on discrete lattices. We attribute this to the inclusion of correlation effects within our approach, since unrestricted Hartree-Fock theory cannot account for skyrmions as self-consistent solutions (or local minima of energy). Indeed it has been also observed by the authors of Ref. [9] that within the tJ-model a semiclassical description cannot account for the occurence of skyrmions but that it is the quantum fluctuations which stabilize this texture. Considering the formation of elliptical domain walls it turned out that these structures only appear for half-filled walls in the low doping regime. Similar to the collinear stripes they are stabilized by a quadrupling of the period along the wall. This can be realized either by alternating on-wall spin currents (Fig. 5a) or by forming a vortex-antivortex structure (Fig. 5b).

ACKNOWLEDGMENTS

We would like to thank V. Hizhnyakov for valuable discussions and a critical reading of the manuscript.

APPENDIX:

Our purpose is to calculate the matrix elements of the hopping matrices $\mathbf{z}_i$ by transforming to a diagonal representation of the matrix $\mathbf{p_i}$ (Eq. (2)) according to

$$T(\mathbf{p_i}) \hat{=} \chi_\mathbf{i}{}^{-1}\mathbf{p_i}\chi_\mathbf{i} = \begin{pmatrix} \lambda_i^+ & 0 \\ 0 & \lambda_i^- \end{pmatrix} \tag{A1}$$

where the eigenvalues are given by $\lambda_i^\pm = \frac{1}{2}(p_{i,\uparrow} + p_{i,\downarrow}) \pm \frac{1}{2}\sqrt{(p_{i,\uparrow} - p_{i,\downarrow})^2 + 2(p_{i,x}^2 + p_{i,y}^2)}$. The transformation matrix χ_i reads as

$$\chi_i = \begin{pmatrix} \alpha_i^+ & \alpha_i^- \\ \beta_i^+ & \beta_i^- \end{pmatrix} \tag{A2}$$

$$\alpha_i^\pm = -\frac{1}{\sqrt{2}}\frac{p_{i,x} - ip_{i,y}}{\sqrt{(p_{i,\uparrow} - \lambda_i^\pm)^2 + p_i^2/2}} \tag{A3}$$

$$\beta_i^\pm = \frac{p_{i,\uparrow} - \lambda_i^\pm}{\sqrt{(p_{i,\uparrow} - \lambda_i^\pm)^2 + p_i^2/2}} \tag{A4}$$

Applied to the hopping matrix this transformation yields

$$\begin{aligned} \mathbf{z}_i &= \chi_\mathbf{i} T(\mathbf{z_i})\chi_\mathbf{i} \\ T(\mathbf{z_i}) &= T(\mathbf{L_i})[e_i T(\mathbf{p_i}) + T(\tilde{\mathbf{p}}_\mathbf{i})d_i]T(\mathbf{R_i}) \end{aligned} \tag{A5}$$

and since $T(\mathbf{p_i})$ is diagonal it is straightforward to evaluate $T(\mathbf{L_i}), T(\mathbf{R_i})$ and $T(\tilde{\mathbf{p}}_\mathbf{i})$ as

$$T(\mathbf{L_i}) = \begin{pmatrix} \frac{1}{\sqrt{1-d_i^2-(\lambda^+)^2}} & 0 \\ 0 & \frac{1}{\sqrt{1-d_i^2-(\lambda^-)^2}} \end{pmatrix} \tag{A6}$$

$$T(\mathbf{R_i}) = \begin{pmatrix} \frac{1}{\sqrt{1-e_i^2-(\lambda^-)^2}} & 0 \\ 0 & \frac{1}{\sqrt{1-e_i^2-(\lambda^+)^2}} \end{pmatrix} \tag{A7}$$

$$T(\tilde{\mathbf{p}}_\mathbf{i}) = \begin{pmatrix} \lambda^- & 0 \\ 0 & \lambda^+ \end{pmatrix} \tag{A8}$$

[1] G. Seibold, E. Sigmund, and V. Hizhnyakov, Phys. Rev. B**57**, 6937 (1998).
[2] M. Fleck, A. I. Liechtenstein, A. M. Oleś, L. Hedin, and V. I. Anisimov, Phys. Rev. Lett. **80**, 2393 (1998).
[3] R. Frésard, and P. Wölfle, J. Phys. C**4**, 3625 (1992).
[4] J. A. Vergés, E. Louis, P. S. Lomdahl, F. Guinea, and A. R. Bishop, Phys. Rev. B**43**, 6099 (1991).
[5] J. Zaanen and O. Gunnarsson, Phys. Rev. B**40**, 7391 (1989).
[6] A. A. Belavin, and A. M. Polyakov, JETP Lett. **22** (10) 245 (1975).
[7] B. I. Shraiman, E. D. Siggia, Phys. Rev. Lett. **61**, 467 (1988).
[8] R. J. Gooding, Phys. Rev. Lett. **66**, 2266 (1991).
[9] S. Haas, F-C. Zhang, F. Mila, T. M. Rice, Phys. Rev. Lett. **77**, 3021 (1996).
[10] J. M. Tranquada, D. J. Buttrey, V. Sachan, and J. E. Lorenzo, Phys. Rev. Lett. **73**, 1003 (1994); J. M. Tranquada, B. J. Sternlieb, J. D. Axe, Y. Nakamura, and S. Uchida, Nature **375**, 561 (1995); J. M. Tranquada, J. D. Axe, N. Ichikawa, A. R. Moodenbaugh, Y. Nakamura, and S. Uchida, Phys. Rev. Lett. **78**, 338 (1997).
[11] J. M. Tranquada, J. D. Axe, N. Ichikawa, Y. Nakamura, S. Uchida, and B. Nachumi, Phys. Rev. B**54**, 7489 (1996).
[12] J. Zaanen and P. B. Littlewood, Phys. Rev. B**50**, 7222 (1994); Z. G. Yu, J. Zang, J. T. Gammel, and A. R. Bishop, Phys. Rev. B**57**, 3241 (1998).
[13] J. Zaanen and M. Oleś, Ann. Physik **5**, 224 (1996).
[14] G. Seibold, C. Castellani, C. Di Castro, and M. Grilli, cond-mat/9803184.
[15] S. R. White and D. J. Scalapino, cond-mat/9705128; S. R. White and D. J. Scalapino, Phys. Rev. Lett. **80**, 1272 (1998).
[16] O. Zachar, S. A. Kivelson, and V. J. Emery, Phys. Rev. B**57**, 1422 (1998).
[17] T. Li, P. Wölfle, and P. J. Hirschfeld, Phys. Rev. B**40**, 6817 (1989); R. Frésard, and P. Wölfle, Int. J. Mod. Phys. B**6**, 237 (1992).
[18] G. Kotliar and A. E. Ruckenstein, Phys. Rev. Lett. **57**, 1362 (1986).